2024 Spring Technical Meeting of the Central States Section of the Combustion Institute
May 12 - 14, 2024
Case Western Reserve University in Cleveland, OH

Flame Characteristics of Ammonia-Dimethyl Ether Blends at High Gas Temperature and Pressure

Tushar Goyal¹ and Omid Samimi-Abianeh^{1,*}

¹Department of Mechanical Engineering, Wayne State University, 5050 Anthony Wayne Dr, Detroit, Michigan, 48202, USA *Corresponding Author Email: o.samimi@wayne.edu

1. Introduction

The escalating severity of climate change necessitates the exploration of alternative fuels for power and propulsion systems to mitigate emissions [1]. Ammonia (NH₃), a renewable and sustainable fuel source, has emerged as a promising candidate to replace conventional fossil fuels due to its high hydrogen content, clean burning nature (producing nitrogen and water upon complete combustion), and established infrastructure for storage and transportation [2]. However, NH₃'s inherently low flame speed presents a significant challenge for widespread practical applications. Prior research revealed several effective approaches to increasing ammonia's combustion characteristics [2,3]. For example, inlet thermodynamic variation, specifically increasing the oxygen content within the fuel mixture, demonstrably accelerates the laminar burning velocity [4– 6]. This is attributed primarily to the thermal effect, leading to the production of radicals and faster flame propagation. Additionally, manipulating the initial temperature has been shown to be effective in boosting both the flame speed and the flammability range of ammonia/air mixtures, thereby broadening the operational window for efficient ammonia combustion [7]. Another potential approach explored in the literature is nonequilibrium plasma-assisted combustion as a flame enhancer [8]. While both preheating temperature and plasma treatment contribute positively, the former appears to have a more pronounced effect due to the change in densities of unburned gases. Blended combustion, a commercially viable strategy involving the introduction of highdiffusivity fuels like hydrogen or methane into the ammonia mixture has also been investigated [9]. Studies indicate that hydrogen addition promotes favorable reaction pathways, leading to a significant increase in flame speed. However, the addition of methane in ammonia has been shown to have a detrimental effect on the burning velocity [10].

Building upon these findings, the present study investigates flame characteristics of ammonia/dimethyl ether (NH₃/DME) blends under autoignitive conditions. The rapid compression machine-flame (RCM-Flame) setup [11] was employed to measure the laminar flame speeds of stoichiometric NH₃/DME mixtures in oxygen-nitrogen-argon flames at the end of compression pressure of 5 bar across a wide elevated temperature range. This data aims to bridge the knowledge gap in NH₃/DME flame characteristics and provide high-fidelity data for refining chemical kinetic models for NH₃/DME blend, ultimately optimizing them as a viable alternative fuel source.

2. Methodology and Experimental Setup

2.1. Rapid compression machine-flame (RCM-Flame) facility

The NH₃/DME flame experiments were conducted in a stainless steel RCM-Flame combustion chamber with a nominal inner diameter of 5.08 cm and a stroke length of 25.4 cm. A schematic of the RCM-Flame setup is shown in Fig. 1. The creviced piston [12] was pneumatically driven and hydraulically stopped. A 0.75-inch thick, and 2-inch diameter sapphire window provided optical access, limiting operating conditions to 250 bar and 1100 K after the end of compression (EOC). A detailed description and validation of the RCM-Flame method can be found in our previous work [11].

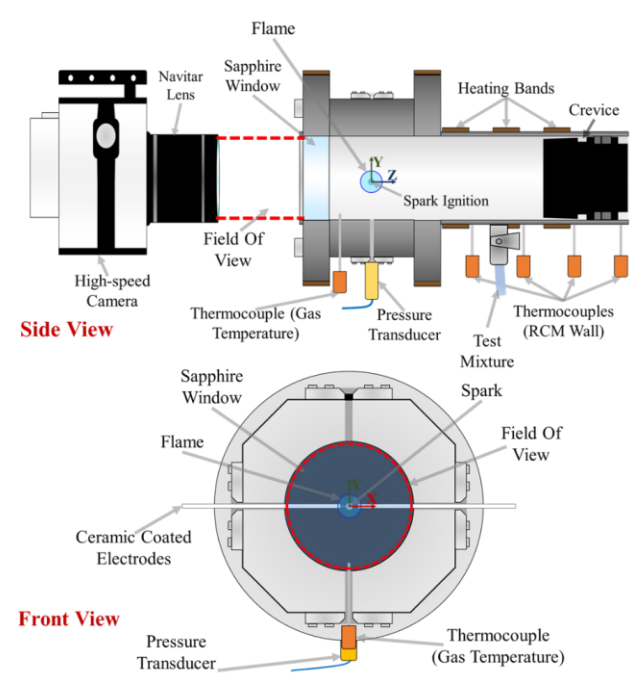


Figure 1. RCM-Flame schematic with high-speed imaging and spark energy release system. The electrodes are placed 11.54 mm from the sapphire window.

Reactant mixtures were prepared in a 5-gallon stainless-steel vessel using Dalton's partial pressure method with a high-accuracy pressure sensor (Omega, PX409-050A10V-EH) to minimize the equivalence ratio uncertainties. Gas components (ammonia, oxygen, nitrogen, argon) were research grade (99.9999%) from Airgas; Dimethyl ether (99.5%) was chemically pure from BVV. The vessel was evacuated to sub-atmospheric pressure (2 mbar) before sequential components were introduced. The details of the mixture compositions are summarized in Table 1.

Table 1: Test Mixture Compositions¹

Mixture Number	D_R	Mixture Composition				
		Ar	N ₂	O_2	NH ₃	DME
1	D_{30}	0.6885	-	0.1830	0.0899	0.0385
2		0.6197	0.0689			
3		0.5508	0.1377			
4		0.4820	0.2066			

¹ Partial pressure of the mixture are reported in bar

-

The initial gas pressure and temperature were measured before each experiment using the aforementioned pressure sensor and a high-accuracy K-type thermocouple (Omega, KMQSS-125G-6), respectively. The chamber wall temperatures were monitored using five K-type thermocouples (Omega, KMQSS-062G-6) to ensure temperature homogeneity. An oil-filed, fast-response piezoelectric pressure transducer (Kistler, 6045B) measured the time-resolved gas pressure coupled with a charge amplifier (Kistler, 5018). The data was recorded using an in-house LabVIEW program. The isentropic compression equation was employed to calculate pre- and post-compression gas temperatures. The accuracy of Eq.(1)² is well discussed in previous works [13]. A homogeneous batch reactor model (HBR) from Chemkin-Pro [14] was used to solve the isentropic equation. The chemistry was assumed frozen during the compression stroke and is not valid for very short ignition delay times (in the order of 1-3 ms).

$$\ln\left(\frac{P}{P_i}\right) = \int_{T_i}^{T} \frac{\gamma(T)}{\gamma(T) - 1} \frac{dT}{T} \tag{1}$$

2.2. Autoignition-assisted flame speed measurements

The autoignition-assisted flames were initiated after the end of compression using a spark energy control system. The system included two opposing centrally located horizontal nickel-copper electrodes (spark gap: 1.016 mm, diameter: 1.01 mm) coated with ceramic. The spark discharge to these electrodes was regulated using a variable voltage supply (TekPower, TP3015E), a solid-state relay (VB Controls, PE0630), an ignition coil (MSD Ballast 2), laser (Calpac Laser, CP-TIM-201-1D-650, 630-680 nm), Silicon photodiode (Hamamatsu, S#1787-08), and a delay generator (Stanford Research Systems, DG646).

Flame growth images were recorded through a sapphire window. The images were acquired at 10kHz using a camera (Vision Research, Phantom VEO 410L). A variable focal length lens (Navitar, DO-5095) was used to focus the camera at the location of the flame initiation, 11.54 cm from the sapphire window. The resulting field of view was 256 × 256 pixel window. The camera and the spark energy control system received one pulse each upon the signal getting disrupted once the piston was released. A detailed explanation of the methodology used to interpret the flame images can be found in previous publications (e.g., [11,15]). However, a succinct overview of the process will be provided here. A multiple-level Otsu method was used to binarize each image and a boundary method [16] was used to detect the edges of each binarized image. To obtain a pixel-to-cm scalar, a known physical dimension was multiplied (i.e., (bore diameter/effective pixels across the 2D plane of the sapphire window).

Flame propagation relative to the burned gas and elliptical symmetry was assumed along the perpendicular axis of electrodes, and instantaneous burning velocity (S_b) and curvature (κ) were calculated by local, instantaneous radius along the axis of symmetry. The unstretched, burned flame speed (S_b^0) was extrapolated from the burned flame speed (S_b) vs. stretch rate (κ/S_b) data using the non-linear stretch model originally proposed by Ronney and Sivashinsky [17]: $\ln(S_b) = \ln(S_b^0) - S_b^0 L_b \kappa/S_b$. Here, L_b is the Markstein length. The maximum flame radius used for flame speed determination was limited by either the onset of instabilities (indicated by a late-time rise in S_b) or confinement effects (indicated by a late-time decrease in S_b). In all experiments, the maximum flame radius used for fitting was less than 35.4% of the inner radius of the RCM-Flame

 $^{^{2}\}gamma$, T_{i} , T, P_{i} and P are defined as specific heat ratio, initial temperature, instantaneous temperature, initial gas pressure, and instantaneous gas pressure, respectively.

- a metric suggested by Burke et al. [18], and validated in our previous publications [11,15] to avoid the influence of confinement effects.

3. Results and Discussion

Measurements of NH₃/DME autoignition-assisted flame speeds were conducted in oxygen-nitrogen-argon mixtures at an equivalence ratio of 1.0. The end of compression pressure was 5 bar, and the gas temperature ranged between 625 and 664 K.

Figure 2 shows the measured stretched burning velocity plotted against the stretch rate at a pressure of 5 bar using mixtures #1-4 (as detailed in Table 1) and four gas temperatures. The flame post-processing duration is bounded by a red-shaded area, with lower and upper limits of 4.5 and 7.35 mm. A linear relation between burning velocity and stretch rate is observed for all studied cases, with burning velocity increasing with gas temperature. The burning velocity also increases with increasing stretch rate, indicating resistance to stretch-induced acceleration. Negative Markstein lengths are observed at all gas temperatures except 664 K, suggesting that the laminar flame speed is slightly affected by instabilities and is approaching potential flame extinction.

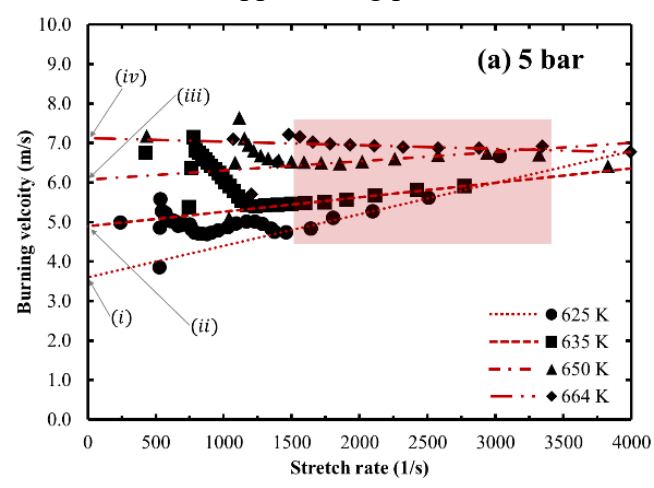


Figure 2. The plots depict the relationship between stretched burning velocity (S_b^0) and stretch rate (κ) using mixture #1 – 4. The data are illustrated by linear extrapolation. The zero-stretch rate burning velocities (S_b^0) for 5 bar are (i) 3.59, (ii) 4.89, (iii) 6.07, and (iv) 7.12 m/s.

Figure 3 presents the measured pressure-time profiles of reactive and non-reactive mixtures at 5 bar. Comparing the reactive and non-reactive profiles reveals heat releases in the reactive mixture. The measured first-stage and total ignition delay times (in ms) decrease with increasing gas temperature. The reactive mixture pressure-time profile closely follows the non-reactive mixture profile until the first-stage ignition delay.

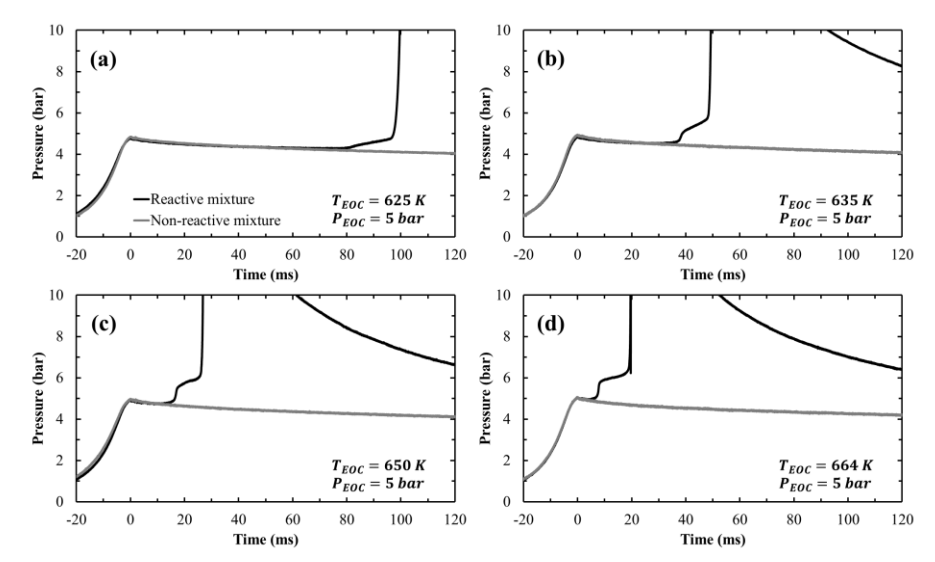


Figure 3. Measured reactive and non-reactive mixture pressure profiles. The reference point of time '0' ms corresponds to the end of compression conditions.

The beta-Damköhler Number (β -D.N.), a non-dimensional number, is introduced to quantify the mixture composition before and after the first-stage ignition delay time in the observed two-stage ignition phenomenon. β -D.N. is defined as the ratio of spark initiation time to the first-stage ignition delay time, as shown in Eq. (1). A β -D.N. below one indicates that the spark is initiated before the first-stage ignition delay, while a value above one signifies that the spark is initiated after the first-stage ignition delay.

$$\beta\text{-D.N.} = \frac{\textit{time of spark initiation}}{\textit{first-stage ignition delay time}} \tag{1}$$

The effect of β -D.N. on the flame speeds at a pressure of 5 bar and various gas temperatures are shown in Fig. 4. The first-stage ignition delay is indicated by the gray-shaded area, corresponding to β -D.N. of 1.0. The black-solid and black-hollow symbols represent the measured and simulated laminar flame speeds, with their respective uncertainty shown by error bars. Nearly constant flame speeds are observed for β -D.N. is less than 1.0, with a slight increase for higher values due to increased gas temperature and pressure after the first-stage ignition delay. Simulations underpredict the measured data but agree with the measurements' uncertainty. The maximum uncertainties of the measured laminar flame speed are 6.54%, 7.34%, 13.22%, and 15.93% and the average differences between the measured and simulated data depend on the gas temperature.

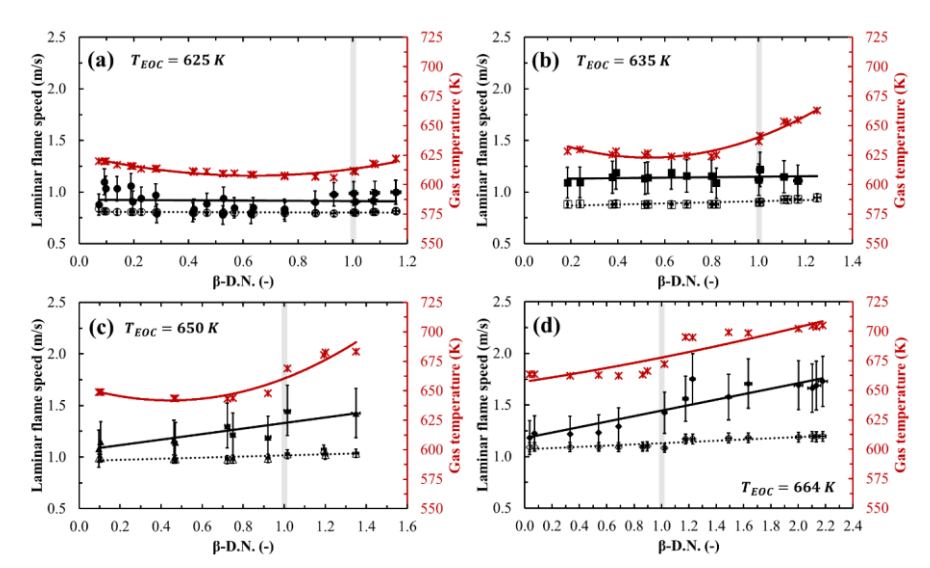


Figure 4. Measured (black-solid symbols) and simulated (black-hollow symbols) laminar flame speed as a function of β -D.N. The end of compression pressure is 5 bar.

4. Conclusions

Autoignition-assisted flame speed measurements were conducted for 90%NH₃/10%DME blend at the end of compression pressure of 10 bar. Linear stretch correlation is used to account for both stretch and curvature effects while deducing flame speeds from high-speed flame images. The results show an increase in flame speed with increasing gas temperature. The laminar flame speeds were found to be constant before β -D.N. equals one. A slight increase is observed in laminar flame speed as the β -D.N. exceeded one due to an increase in pressure and temperature observed after the first-stage ignition delay.

5. Acknowledgements

This work is supported by the National Science Foundation, United States, under Grant No. 2324471. Any opinions, findings, conclusions, or recommendations expressed in this material are those of the authors and do not necessarily reflect the views of the National Science Foundation.

6. References

- [1] ICAO Secretariat. ICAO Environmental Report 2022. 2022.
- [2] Valera-Medina A, Xiao H, Owen-Jones M, David WIF, Bowen PJ. Ammonia for power. Prog Energy Combust Sci 2018;69:63–102. https://doi.org/10.1016/j.pecs.2018.07.001.
- [3] Kobayashi H, Hayakawa A, Somarathne KDKA, Okafor EC. Science and technology of ammonia combustion. Proc Combust Inst 2019;37:109–33. https://doi.org/10.1016/j.proci.2018.09.029.
- [4] Shrestha KP, Lhuillier C, Barbosa AA, Brequigny P, Contino F, Mounaïm-Rousselle C, et al. An experimental and modeling study of ammonia with enriched oxygen content and ammonia/hydrogen laminar flame speed at elevated pressure and temperature. Proc Combust Inst 2021;38:2163–74. https://doi.org/10.1016/j.proci.2020.06.197.
- [5] Mei B, Zhang X, Ma S, Cui M, Guo H, Cao Z, et al. Experimental and kinetic modeling investigation on the laminar flame propagation of ammonia under oxygen enrichment and elevated pressure conditions. Combust Flame 2019;210:236–46. https://doi.org/10.1016/j.combustflame.2019.08.033.
- [6] Li J, Huang H, Kobayashi N, He Z, Osaka Y, Zeng T. Numerical study on effect of oxygen

- content in combustion air on ammonia combustion. Energy 2015;93:2053–68. https://doi.org/10.1016/j.energy.2015.10.060.
- [7] Han X, Wang Z, He Y, Liu Y, Zhu Y, Konnov AA. The temperature dependence of the laminar burning velocity and superadiabatic flame temperature phenomenon for NH3/air flames. Combust Flame 2020;217:314–20. https://doi.org/10.1016/j.combustflame.2020.04.013.
- [8] Kondo S, Takizawa K, Takahashi A, Tokuhashi K. On the temperature dependence of flammability limits of gases. J Hazard Mater 2011;187:585–90. https://doi.org/10.1016/j.jhazmat.2011.01.037.
- [9] Li J, Huang H, Kobayashi N, Wang C, Yuan H. Numerical study on laminar burning velocity and ignition delay time of ammonia flame with hydrogen addition. Energy 2017;126:796–809. https://doi.org/10.1016/j.energy.2017.03.085.
- [10] Xiao H, Valera-Medina A, Bowen PJ. Study on premixed combustion characteristics of cofiring ammonia/methane fuels. Energy 2017;140:125–35. https://doi.org/10.1016/j.energy.2017.08.077.
- [11] Goyal T, Samimi-Abianeh O. Measurement and Simulation of Autoignition-Assisted Flame Speed of N -Heptane Mixture at Elevated Gas Temperature. Ind Eng Chem Res 2023;62:8719–25. https://doi.org/10.1021/acs.iecr.3c01102.
- [12] Mittal G, Sung CJ. Aerodynamics inside a rapid compression machine. Combust Flame 2006;145:160–80. https://doi.org/10.1016/j.combustflame.2005.10.019.
- [13] Piehl JA, Samimi-Abianeh O. Measuring the Adiabatic Ignition Delay of n-Pentane Mixture using Rapid Compression Machine. J Therm Sci 2020. https://doi.org/10.1007/s11630-020-1346-7.
- [14] ANSYS I. CHEMKIN-PRO 2020 R2, Theory Manual 2020.
- [15] Goyal T, Samimi-Abianeh O. Methane Laminar Flame Speed Measurement at High Gas Temperature Using Rapid Compression Machine-Flame (RCM-Flame). Ind Eng Chem Res 2022;61:9981–90. https://doi.org/10.1021/acs.iecr.2c01117.
- [16] Taubin G. Estimation of Planar Curves, Surfaces, and Nonplanar Space Curves Defined by Implicit Equations with Applications to Edge and Range Image Segmentation. IEEE Trans Pattern Anal Mach Intell 1991;13:1115–38. https://doi.org/10.1109/34.103273.
- [17] Ronney PD, Sivashinsky GI. A Theoretical Study of Propagation and Extinction of Nonsteady Spherical Flame Fronts. SIAM J Appl Math 1989;49:1029–46. https://doi.org/10.1137/0149062.
- [18] Burke MP, Chen Z, Ju Y, Dryer FL. Effect of cylindrical confinement on the determination of laminar flame speeds using outwardly propagating flames. Combust Flame 2009;156:771–9. https://doi.org/10.1016/j.combustflame.2009.01.013.